THE ASTROPHYSICAL JOURNAL, 375:704–715, 1991 July 10

THE MANY FACES OF F STARS: A ROTATIONAL MODULATION STUDY OF CAPELLA, PROCYON, AND CAPH WITH THE *INTERNATIONAL ULTRAVIOLET EXPLORER*

THOMAS R. AYRES[1]
Center for Astrophysics and Space Astronomy, Campus Box 391, University of Colorado, Boulder, CO 80309-0391
Received 1990 October 10; accepted 1991 January 4

ABSTRACT

I monitored the far-ultraviolet emissions of three bright "F" stars—the Capella secondary (α Aur Ab: G0 III), Procyon (α CMi A: F5 IV–V), and Caph (β Cas: F2 III–IV)—over one or more rotational cycles with the *International Ultraviolet Explorer*. Strong rotational modulations produced by isolated "active regions" are a characteristic signature of the hydromagnetic dynamo, believed to be the root of the nonclassical hot outer atmospheres—chromospheres and coronae—of late-type stars.

Although all three stars are regarded as chromospherically "active" (with C IV λ1549 surface flux densities up to 20 times solar), none exhibited any sensible rotational modulations, even at the high sensitivity achieved by pseudo-trailing low-dispersion spectra on the SWP camera (precisions of 2%–5% [1 σ] in key emission lines and 0.5%–1.6% in reference continuum bands). The only significant cyclical variation was in the 1500 Å continuum of Caph, associated with its 0.1 day δ Scuti pulsation. (However, I found no evidence that H I λ1216 is persistently enhanced near minimum light, contrary to the suggestion of Teays et al. for Mg II λ2800.)

The lack of rotational modulations indicates a smooth surface distribution of chromospheric emission, in sharp contrast to the *active longitudes* of later type coronal stars ranging from "quiet" dwarfs like the Sun to the hyperactive RS CVn variables. Balancing their unanimously nonsolar behavior with regard to rotational modulations are a variety of puzzling differences among the three F stars revealed by 0.1 Å resolution *IUE* echelle spectra. On the one hand, the C IV features of Procyon are narrow, while those of the Capella secondary and Caph are broad: differences in $v \sin i$ alone cannot explain the dichotomy. On the other hand, the high-excitation emissions of both the Capella secondary and Procyon, but not Caph, exhibit statistically significant *redshifts*: the associated gas flows are common among the cooler dwarfs and giants, and are thought to derive from vertically extensive structures like the magnetic loops of the solar corona.

I discuss the significance of these results in light of the speculation by Simon & Drake that the X-ray-deficient coronae of the early F dwarfs are produced by classical acoustic heating, in contrast to the magnetic-dominated coronae of cooler stars.

Subject headings: stars: chromospheres — stars: emission-line — stars: individual (α Aurigae, α Canis Minoris, β Cassiopeiae) — stars: rotation — ultraviolet: spectra

1. INTRODUCTION

Magnetism is at the heart of a dazzling array of electrodynamic phenomena in the solar chromosphere and corona (Beasley & Cram 1990): the extension of the clear example of the Sun to other stars requires only a small leap of faith. Broad surveys of ultraviolet and X-ray emission in the early 1980s by the *International Ultraviolet Explorer* and *Einstein* strengthened the belief that the hot outer atmospheres of cool stars are energized by magnetic activity (e.g., Jordan & Linsky 1987).

In recent years, however, detailed studies of the early F stars (e.g., Walter 1983; Wolff, Boesgaard, & Simon 1986) have challenged the modern paradigm that virtually all activity has a purely magnetic origin. The empirical studies have revealed profound differences between the behaviors of main-sequence stars on either side of a dividing line in the Hertzsprung-Russell diagram near $B-V \approx 0.42$, as most recently enumerated by Simon & Drake (1989, hereafter SD).

On the one hand, stars to the red of the boundary occupy a broad band of chromospheric and coronal emission levels, in which the surface flux densities are well correlated with the Rossby number (a ratio of rotational and convective time scales: see, e.g., Noyes et al. 1984). That is a sure sign, some believe, of the operation of the *dynamo*, a convective engine catalyzed by rotation which is responsible for the production of magnetic flux in the outer envelopes of cool stars (Parker 1970).

On the other hand, the stars to the blue of the boundary exhibit high—but much more uniform—levels of ultraviolet and X-ray emission, with little if any correlation with rotation period. SD speculate that solar-like predominantly magnetic behavior occurs to the red side of the boundary, while the previously abandoned classical acoustic heating mechanism (e.g., Ulmschneider 1979) operates to the blue.

In the spirit of exploring the acoustic/magnetic dichotomy from a somewhat different point of view, I conducted a low-dispersion monitoring campaign with the *IUE* to examine three superficially very different stars that SD place on or to the blue of the putative boundary: the yellow giant Capella; the F subgiant Procyon; and the δ Scuti variable Caph. My objectives were to assess (1) whether strong rotational modulations—a clear signature of inhomogeneous magnetic surface activity—are present in the far-ultraviolet emissions of such stars, and (2) whether episodic heating is important in the subcoronal layers of a representative pulsationally unstable star.

[1] Guest Observer with the *International Ultraviolet Explorer* satellite.

2. OBSERVATIONS

2.1. *The Program Stars*

Table 1 summarizes the physical properties and estimated rotational time scales of the program stars. I discuss these in detail below.

2.1.1. *Capella*

Capella (α Aurigae A: G8/K0 III [Aa] + G0 III [Ab]: Bagnuolo & Sowell 1988) is a 104 day spectroscopic binary consisting of a rare combination of a postflash giant (the primary) and a Hertzsprung gap star (the secondary). The ultraviolet emissions of the system are dominated by the fast-rotating secondary (Ayres & Linsky 1980). Its surface flux density of C IV λ1549 is about 20 times that of the Sun.

A previous study of Capella, at high dispersion with the *IUE*, revealed that the ultraviolet emissions from Mg II λ2800 to C IV were remarkably steady over the half orbital cycle (52 days) sampled with a resolution as good as 2 days (Ayres 1984). The 1 σ standard deviations of the time series ranged from 4% for Mg II to 7% for C IV, consistent with the estimated precision of the *IUE* spectroscopy. The constancy of Capella stands in sharp contrast to the behavior of the other major class of "hyperactive" late-type stars: the low-mass ($\gtrsim 1\ \mathcal{M}_\odot$) RS CVn–type binaries (e.g., Linsky 1988 and references therein). The K0 subgiants of the RS CVn systems display sporadic variations in their ultraviolet emissions of factors of 2 on time scales of days; occasionally *flare* by factors of 5–10 on short time scales (hours); and exhibit periodic modulations of their fluxes on rotational time scales (typically less than 20 days) owing to the presence of "active longitudes" where the ultraviolet emissions are particularly intense.

Although the secondary of Capella has been offered as a paradigm of the rotation–magnetic-activity connection (e.g., Ayres & Linsky 1980), SD argue that it is only accidentally so, emphasizing the substantial logarithmic X-ray deficiency ($\Delta R_X = -1.0$ in the authors' notation) of the yellow giant with respect to its large C IV surface flux density (see also Ayres, Schiffer, & Linsky 1983b). SD propose that the extension of the acoustic/magnetic boundary intersects the giant branch near $B-V = 0.7$, just to the red of the Capella secondary.

On the other hand, Rucinski (1986) has reported that optical radial velocity spectra of Capella display a low-amplitude modulation superposed on the orbital velocity curve, with a time scale commensurate with the estimated rotation period of the secondary (about 10 days). Rucinski interpreted the possible modulation as a systematic distortion of the reference absorption profiles arising from an uneven distribution of starspots over the surface of the secondary. If confirmed, it would be compelling evidence for the operation of a solar-like dynamo in the Hertzsprung gap star, contrary to the arguments in favor of the acoustic scenario presented by SD.

2.1.2. *Procyon*

Procyon (α Canis Minoris A: F5 IV–V) is the nearest and brightest of the F stars. It has served as a prototype in many studies, particularly in semiempirical modeling of photospheric and chromospheric properties (Ayres 1975; Ayres, Linsky, & Shine 1974). Procyon's surface flux density of C IV is about 5 times that of the Sun (Ayres, Marstad, & Linsky 1981), and its X-ray deficiency is similar to that of the Capella secondary. The projected rotational velocity of Procyon is only about 3 km s^{-1} (Smith 1979), but the equatorial rotation rate could be 5 km s^{-1} or more based on estimated inclinations of the star (Gray 1981). Owing to the carefully measured orbital properties of the Procyon system (Strand 1951: α CMi B is an 11th magnitude DF white dwarf) and the accurate parallactic distance, the physical properties—mass, luminosity, surface temperature, and radius—are well known. With $B-V = 0.42$ Procyon straddles the proposed acoustic/magnetic boundary: SD consider it a borderline case. Nevertheless, its large X-ray deficiency is characteristic of the early F main-sequence stars on the "acoustic" side.

2.1.3. *Caph*

The resurgence of interest in the acoustic heating mechanism has focused renewed attention on those stars whose envelopes are unstable to moderate-amplitude global pulsations. Two decades ago Kraft (1957) reported that transient Ca II emission was ubiquitous among classical Cepheids whose periods exceed about 4 days. In a detailed study of the 3.74 day Cepheid RT Aurigae, Hollars (1974) found that the chromospheric Ca II emission peaked near phase 0.9 (i.e., near minimum radius) and was accompanied by weak blueshifted components. Schmidt & Parsons (1984) reported analogous behavior in the 2800 Å resonance lines of Mg II in classical Cepheids. Dravins, Lind, & Särg (1977) tentatively identified transient Ca II components in the 0.14 day δ Sct variable ρ Puppis; Fracassini et al. (1983) noted an increase in the Mg II emission of that star near maximum light; Ayres & Bennett (1987) reported a factor of 2 increase in the H I λ1216 Lyα emission of the δ Sct variable Caph (β Cassiopeiae: F2 III–IV) during a 3.5 hr sequence of *IUE* low-dispersion spectra; and

TABLE 1

STELLAR PARAMETERS AND ROTATIONAL TIME SCALES

Parameter	Capella Ab	Procyon	Caph	References
Spectral type	G0 III	F5 IV–V	F2 III–IV	1, 2, 2
$B-V$ (mag)	+0.6	+0.42	+0.34	3, 2, 2
f_{bol} (10^{-7} ergs cm^{-2} s^{-1})	135	180	30	4, 5, 5
$\mathcal{R}/\mathcal{R}_\odot$	9	2.2	2.9	1, 6, 6
$v \sin i$ (km s^{-1})	36 ± 3	2.8 ± 0.3	50	4, 7, 8
i ($\equiv i_{orbit}$)	137°	36°	?	3, 9
v_{rot} (km s^{-1})	53 ± 4	4.8 ± 0.5	$\gtrsim$50	
P_{rot} (days)	9 ± 1	23 ± 2	$\lesssim$3	

REFERENCES.—(1) Bagnuolo & Sowell 1988; (2) Hoffleit & Jaschek 1982; (3) Ayres & Linsky 1980 and references therein; (4) Ayres 1988 and references therein; (5) Ayres et al. 1981; (6) Gray 1967; (7) Gray 1981; (8) Slettebak et al. 1975; (9) Strand 1951.

TABLE 2

CATALOG OF 1986 OBSERVATIONS

SWP Number (1)	JD 2,446,000+ (2)	Exposure Type (3)	FPM (V) (4)	t_{TFL} (s) (5)	THDA (°C) (6)	$f_L/f_C/f_{BKG}$ (DN) (7)
			A. Capella			
27681.....	469.65	Triple	0.6	3.3	10.5	230/102/68
27696.....	472.53	Single	1.4	3.3	8.5	222/93/67
27700.....	473.57	Triple	1.9	2.6	7.2	211/99/65
27701.....	473.61	Triple	2.1	2.5	7.5	214/98/66
27706.....	474.45	Triple	1.3	3.3	6.8	227/103/72
27711.....	475.45	Triple	1.0	3.3	6.8	235/105/70
27718.....	476.58	Triple	2.5	0.9	8.5	219/94/58
27725.....	477.36	Triple	1.8	2.9	10.8	229/102/68
27729.....	478.34	Triple	1.5	3.3	9.8	240/105/71
27735.....	479.50	Triple	0.7	3.3	10.2	221/104/67
27755.....	482.36	Triple	0.5	3.3	6.8	228/104/71
27756.....	482.40	Triple	0.5	3.3	6.8	230/109/70
27769.....	483.49	Triple	1.0	3.3	7.8	229/109/73
27787.....	486.48	Triple	2.4	0.9	8.5	216/95/59
27802.....	488.49	Triple	2.4	1.3	9.5	229/99/61
27807.....	489.34	Triple	2.0	2.5	8.2	238/101/66
27813.....	490.33	Triple	1.8	2.9	8.5	237/106/68
27835.....	493.33	Triple	2.1	2.5	10.2	233/104/73
27844.....	494.32	Triple	1.0	3.3	9.5	246/103/70
27855.....	495.49	Triple	1.9	2.6	8.8	238/103/65
27860.....	496.47	Triple	0.1	3.3	9.2	237/104/68
			B. Procyon			
27694.....	472.42	Triple	0.7	3.3	8.5	195/67/45
27695.....	472.47	Triple	1.0	3.3	8.5	202/71/46
27702.....	473.68	Triple	0.3	3.3	8.8	210/68/46
27707.....	474.53	Single	2.4	1.7	7.2	192/47/29
27712.....	475.57	Triple	2.6	0.0	6.8	208/63/40
27719.....	476.64	Triple	2.0	2.5	9.2	208/66/42
27720.....	476.69	Triple	0.1	3.3	10.5	206/66/44
27726.....	477.43	Triple	1.9	2.6	10.5	209/66/42
27727.....	477.47	Triple	2.0	2.5	10.5	200/68/44
27730.....	478.40	Triple	1.3	3.3	9.8	218/72/46
27731.....	478.44	Single	1.2	3.3	9.8	196/59/42
27736.....	479.56	Triple	1.9	2.6	10.2	208/64/41
27754.....	482.31	Triple	0.5	3.3	6.8	200/67/45
27770.....	483.54	Triple	1.8	2.6	7.5	206/67/42
27788.....	486.54	Single	2.9	0.9	8.5	181/51/36
27789.....	486.57	Single	3.0	0.0	8.5	187/50/31
27803.....	488.54	Single	2.8	1.7	9.5	188/61/42
27808.....	489.41	Triple	1.8	2.9	8.2	219/71/47
27814.....	490.39	Triple	1.0	3.3	8.8	228/69/46
27815.....	490.44	Triple	1.8	2.9	9.0	220/71/47
27836.....	493.39	Triple	1.9	2.5	10.0	226/66/45
27837.....	493.43	Triple	1.3	3.3	10.0	218/69/46
27845.....	494.39	Triple	1.0	3.3	9.5	219/68/46
27846.....	494.42	Single	1.0	3.3	9.5	187/62/41
27856.....	495.54	Triple	1.9	2.5	8.8	217/68/42
27861.....	496.53	Triple	1.2	3.3	8.8	219/70/45

Col. (2).—Exposure start time.

Col. (3).—"Triple" refers to triple exposure [offset reference points (ORPs): (+05, −212), (−16, −208), and (−37, −204)] with 3^m20^s integration at each ORP. "Single" refers to single exposure (3^m20^s) centered in the large aperture [ORP: (−16, −208)].

Col. (4).—Radiation reading from Fields and Particle Monitor.

Col. (5).—Tungsten filament lamp exposure to yield constant background given radiation fogging during exposure (predicted from FPM).

Col. (6).—Camera temperature recorded at time of read cycle.

Col. (7).—f_L is the peak DN of the emission-line histogram of the $\mathcal{N}$-tuple pseudo-trail, ignoring the $\mathcal{N}$ highest values; f_C and f_{BKG} are the centroids of histograms for the adjacent continuum and off-spectrum background, respectively; the lines are C IV λ1549 for Capella and H I λ1216 for Procyon.

Teays et al. (1989) found phase-dependent emission in the Mg II doublet of Caph, but peaking near *minimum light*, contrary to the behavior cited previously for ρ Pup and the Cepheids.

The episodic heating attributed to pulsations in the Cepheids and δ Sct stars potentially is of great significance in the debate concerning the acoustic/magnetic boundary: in some sense it represents an extreme form of the acoustic mechanism.

Caph is the nearest and brightest of the δ Sct variables (McNamara & Augason 1962), a populous class in the Galaxy (Breger 1979). Its pulsation period is a tenth of a day, and the amplitude is a few hundredths in V (Millis 1966). Recently, Walker & Wolstencroft (1988) have proposed that Caph is surrounded by a β Pic–like dust disk at a distance of about 11 AU. Caph is an intense C IV source with a surface flux density some 20 times solar (Linsky & Marstad 1981), and its rotational velocity is comparable to that of the Capella secondary. With $B-V = 0.35$ and an X-ray deficiency of two orders of magnitude (the largest identified by SD), Caph lies safely on the blue side of the putative boundary.

2.2. *Circumstances of the Present Program*

2.2.1. *Low-Dispersion Monitoring Campaigns*

I observed Capella and Procyon with the *IUE* between 1986 February 7 and March 6: ten 8 hr shifts split into more or less regularly spaced 4 hr blocks. Subsequently, in 1987 October, I observed Caph over a 4 day period, split into two 4 hr blocks, one 8 hr block, and one 12 hr block. Tables 2 and 3 summarize the circumstances of the two observing campaigns.

I conducted both programs during NASA second shifts (US2), which often experience elevated levels of charged-particle radiation. The associated Cherenkov fogging (Harris & Sonneborn 1987) can significantly raise the background counts (in data numbers [DN]) upon which the spectrum sits, and thereby change from day to day the portion of the photometric linearization function that is applied to the emission-line spectrum. Any subtle errors in the linearization procedure potentially could produce an apparent variability of the line emission, even if the source itself were constant.

Thus, for each low-dispersion spectrum of the monitoring campaign, I superposed a short exposure of the tungsten-filament flash lamps (TFL) to maintain a background of ≈ 65 DN (at 1550 Å) in the face of day-to-day differences in the particle radiation levels.

For Capella and Procyon, I took pseudo-trailed triple exposures (3^m20^s for each subimage) designed to yield a peak DN of ≈ 220 at the C IV line of the former and the H I λ1216 Lyα line of the latter, taking into account the elevated background due to the radiation compensation scheme. For the significantly weaker spectrum of Caph, I took double exposures (5^m0^s each) designed to yield a peak DN of ≈ 110 for Lyα.

Figure 1 depicts representative SWP low-dispersion frames of the three stars, based on the photometrically corrected, geometrically rotated and resampled "extended line-by-line" (ELBL) file provided to the Guest Observer.

2.2.2. *SWP Echellogram of Caph*

In conjunction with the Caph monitoring program, I exposed a 500 minute high-dispersion spectrum (SWP 32002) during the US1 shift on 1987 October 5/6 (UT). I placed the target on the major axis of the 10″ × 20″ large aperture about 5″ from the center. Such intentional shifts of the echelle pattern are valuable for moving important emission features—such as O I λ1302.2 and C II λ1334.5—away from unfortunately placed reseau marks, and enhance the success of specialized co-addition schemes like that described by Ayres et al. (1986).

SWP 32002 represents the deepest practical high-dispersion *IUE* exposure of an early F star like Caph. It is heavily over-exposed longward of echelle order 82 ($\lambda > 1670$ Å), owing to the rapidly rising F-type photospheric continuum. Cross-dispersed scattered light is visible down to order 98 ($\lambda \approx 1400$

TABLE 3

CATALOG OF 1987 OBSERVATIONS: CAPH

SWP NUMBER (1)	JD 2,447,000+ Exposure 1 (2)	JD 2,447,000+ Exposure 2 (3)	FPM (V) (4)	t_{TFL} (s) (5)	THDA (°C) (6)	$f_L/f_C/f_{BKG}$ (DN) (7)
31970.....	71.740	71.747	0.4	3.3	9.8	100/52/41
31971.....	71.776	71.784	0.1	3.3	9.8	103/51/41
31972.....	71.813	71.822	0.8	3.3	9.8	110/52/42
31973.....	71.849	71.857	2.2	2.0	9.8	101/47/33
31979.....	72.750	72.757	0.1	3.3	7.5	104/49/41
31980.....	72.787	72.794	0.1	3.3	7.5	114/52/41
31981.....	72.824	72.830	0.3	3.3	7.5	106/52/40
31982.....	72.861	72.869	0.6	3.3	7.5	113/54/41
31983.....	72.898	72.905	1.4	3.3	7.2	117/60/43
31984.....	72.934	72.944	1.7	3.3	7.2	104/57/45
31985.....	72.970	72.977	1.5	3.3	7.2	100/55/44
31986.....	73.005	73.013	0.8	3.3	7.2	107/54/42
31992.....	73.736	73.743	0.4	3.3	7.5	108/55/42
31993.....	73.770	73.777	0.4	3.3	7.5	117/53/41
31994.....	73.804	73.811	0.8	3.3	7.5	110/56/43
31995.....	73.838	73.846	1.3	3.3	7.2	112/59/44
32004.....	74.801	74.807	0.1	3.3	7.8	107/53/40
32005.....	74.836	74.842	1.0	3.3	7.8	122/57/44
32006.....	74.871	74.878	1.5	2.6	7.5	113/53/38
32007.....	74.907	74.913	2.0	2.0	7.5	108/50/36

NOTE.—All observations are double exposures [ORPs: (+05, −212) and (−37, −204)] with 5^m0^s integration at each ORP. Col. (7): H I λ1216.

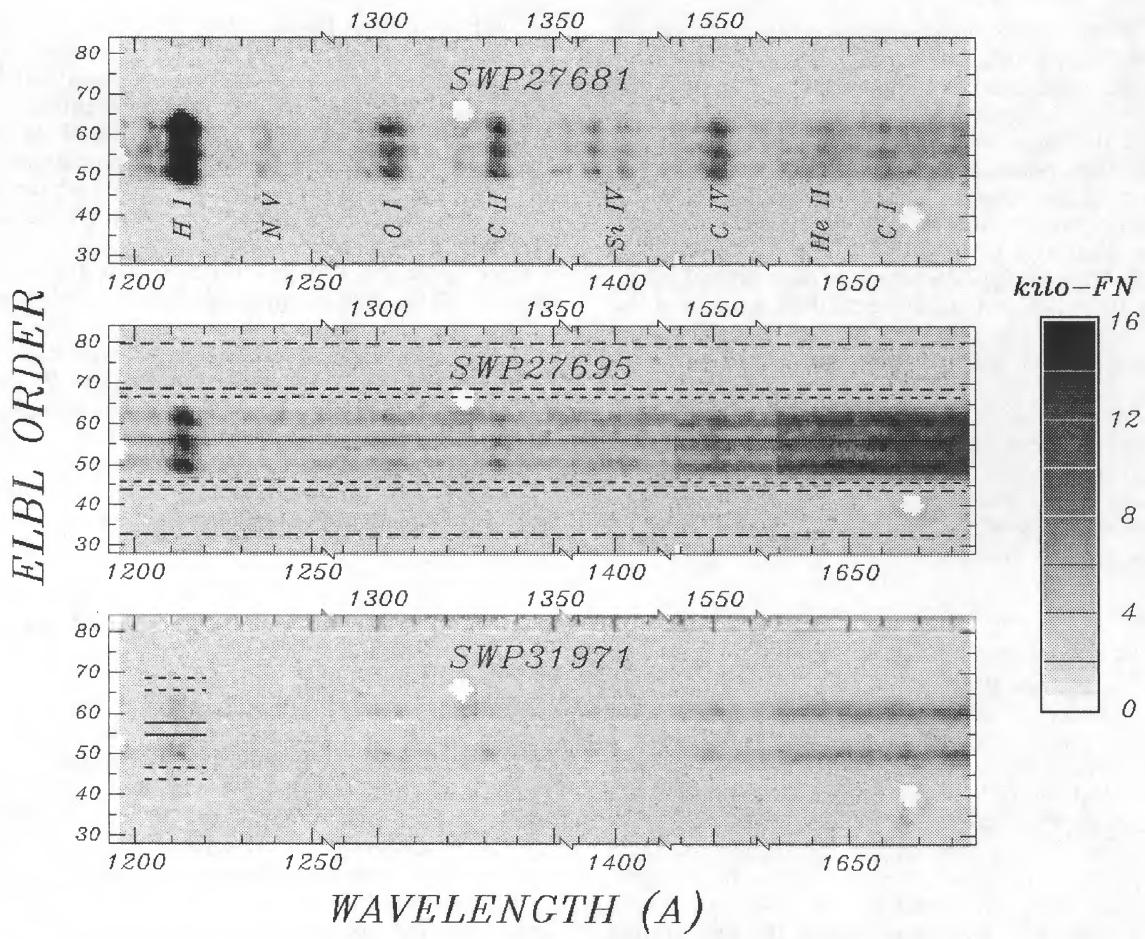

FIG. 1.—Gray-scale depictions of representative SWP low-dispersion spectrograms from the two monitoring campaigns. From top to bottom, the spectra are of Capella, Procyon, and Caph. The observations all are pseudo-trails: triple exposures for Capella and Procyon, and a double exposure for Caph. The images were derived from the photometrically corrected "ELBL" file, with intensities in linearized flux numbers, and have been pieced together in wavelength intervals containing important emission lines (identified explicitly in the upper panel). One ELBL "pseudo-order" corresponds to $\approx 1''.1$. The H I λ1216 emission of Capella is heavily overexposed, as are all of the spectra longward of about 1700 Å. The dashed lines in the middle panel illustrate the extraction zones for the gross flux (central region) and the off-spectrum background (flanking swaths). The shorter dashed lines in the lower panel depict the windows utilized to test for the presence of appreciable geocoronal H I Lyα contamination in the Caph spectra. The irregular white patches highlight areas of the images affected by reseau marks.

Å) and adds significantly to the interorder background. The C IV λ1548.2 component has a peak DN of about 220, somewhat over an optimum exposure of 205 (e.g., Coleman & Snijders 1977). However, the net line intensity is only about 60 DN above the elevated background. H I Lyα appears at about 180 DN over a background of 80, although it is dominated by the geocoronal component: the true stellar peak emission is at least 10 DN less. C II λ1335.7 is recorded at about 50 DN over background.

Table 4 describes the circumstances of SWP 32002, and a sample of earlier exposures of Procyon and Caph which I analyzed for the present study. High-quality reference spectra of Capella have been published by Ayres (1984, 1988) and Ayres et al. (1983b).

Two of the previous echellograms—SWP 26917 and SWP 33945—were exposed (by other observers) through the 3″ diameter small aperture. Its effective throughput can be as large as about 60%, but often is much less. I determined effective transmissions of 40% and 20%, respectively, for the two small-aperture spectra according to the apparent fluxes in a well-exposed 8 Å continuum band near 1650 Å. The abnormally low value for SWP 33945 indicates that the target very likely was entirely out of the aperture for perhaps half the duration of the exposure.

3. REDUCTIONS AND MEASUREMENTS

3.1. *Extraction of Low-Dispersion Multiple Exposures*

I extracted the pseudo-trailed exposures from the "spatially resolved" ELBL files using custom software, which, however, is traceable to standard (*IUE* Regional Data Analysis Facility) procedures and calibration tables. For the triple exposures, I utilized a 22″ extraction slot. It extends somewhat beyond the cross-dispersion width of the pseudo-trailed image to compensate for the $\pm 1''$ undulations in the centroid of the spectrum from 1150 Å to 1700 Å (Altner 1988). I extracted the background intensities in two 11″ swaths beginning 14″ to either side of the center line. Figure 1 illustrates the extraction geometry.

I processed the double exposures of Caph using the same extraction parameters as for the triple exposures of Capella and Procyon. However, I also sampled—and compensated

TABLE 4

CATALOG OF SWP ECHELLE SPECTRA

SWP Number (1)	JD 2,440,000+ (2)	Exposure Type (3)	t_{exp} (minutes) (4)	f_{HI} (10^{-11}) (5)	Observer (6)
		Procyon			
20048.....	5,477.39	L/O	110	12.0	Ayres
21194.....	5,607.74	L/O	60	10.6	Ayres
21195.....	5,607.80	L/O	60	12.1	Ayres
21196.....	5,607.86	L/O	60	14.0	Ayres
26917.....	6,350.10	S/C	200	4.8	HM 133[a]
		Caph			
24127.....	5,979,91	L/O	185	3.0	Ayres
32002.....	7,074.40	L/O[b]	500	2.5	Ayres
33945.....	7,362.68	S/O	772	0.4	Murthy

NOTE.—In col. (3), "L" refers to exposure through large aperture, "S" through small aperture; "/O" indicates that the large-aperture shutter was open; and "/C" indicates that it was closed. Col. (5) gives integrated flux of H I Lyα from echelle order 113 in ergs $cm^{-2} s^{-1}$ at Earth.

[a] Program designation: Vilspa observer not recorded in merged log.

[b] ORP: (+05, −212), equivalent to velocity shift of +26 km s^{-1}.

for—the extended geocoronal Lyα light that more or less uniformly fills the large aperture (see Fig. 1). In only a few cases was the geocoronal contamination large enough to trigger a significant correction.

On a few occasions during the first phase of the program (Capella and Procyon), time constraints dictated a single exposure (centered in the large aperture) instead of a pseudo-trail. I extracted these using a 12″ slot with flanking 6″ background swaths beginning ±9″ from the center line.

3.2. *Measurement of Fluxes in the Low-Dispersion Spectra*

I used a semiautonomous line-finding and -fitting algorithm (Bennett 1987) to measure the fluxes of emission lines and broad continuum bands in the extracted low-dispersion spectra. The numerical procedure ensures uniformity in the measured fluxes. The algorithm includes an automated definition of the "continuum" level against which the emission lines are fitted (with least-squares Gaussians) as described by Bennett & Ayres (1988).

The automated line-fitting routine evaluates uncertainties in the Gaussian line fluxes using the prescription of Landman, Roussel-Dupré, & Tanigawa (1982). The authors' formula is not technically appropriate to the noise characteristics of the SWP camera (Ayres 1990), but it is sufficiently reliable for the present purposes (at worst it underestimates the flux errors by ≈50%).

Figure 2 illustrates the application of the fitting procedure to representative spectra of the three program stars. Table 5 lists

TABLE 5

FITTED EMISSION LINES AND CONTINUUM BANDS

Group[a] (1)	Species and Wavelength[b] (Å) (2)
	Emission Lines
1	C III λ1175.7m
2	Si III λ1206.5, H I λ1215.7
3	N V λ1240.1m
4	S I λ1295.9m, O I λ1304.8m
5	C II λ1335.3m
6	Si IV λ1393.8, Si IV λ1402.8
7	C IV λ1549.1m, C I λ1561.1m
8	He II λ1640.4m, C I λ1657.2m, O III λ1666.2
	Continuum Bands
	1425–1525
	1575–1625
	1675–1725[c]

[a] Lines within a group were fitted by blended Gaussians.

[b] The suffix "m" indicates intensity-weighted mean wavelength of multiplet.

[c] Capella only.

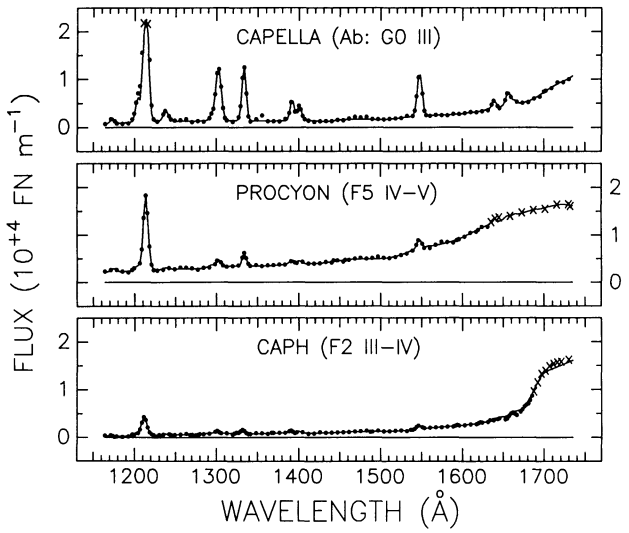

FIG. 2.—Representative extracted spectra of the three program stars, corresponding to the spatially resolved images depicted in Fig. 1. The observed spectra, in uncalibrated flux numbers, are the solid dots, and the fitted spectral traces—as modeled by an automated numerical procedure—are the overlying smooth curves. Crosses mark portions of the spectra that are overexposed. Much of the "continuum" emission of these stars below about 1500 Å is grating-scattered light.

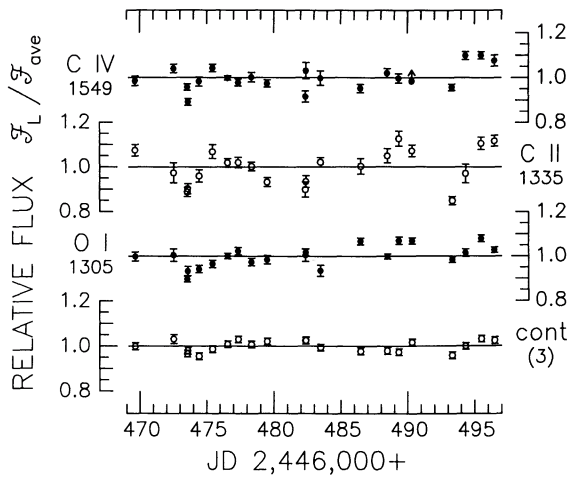

FIG. 3a

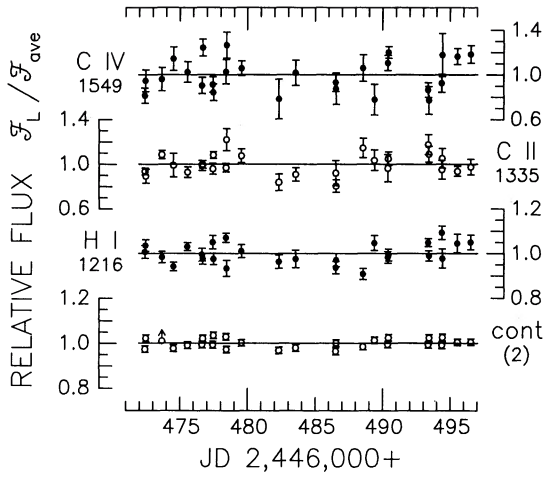

FIG. 3b

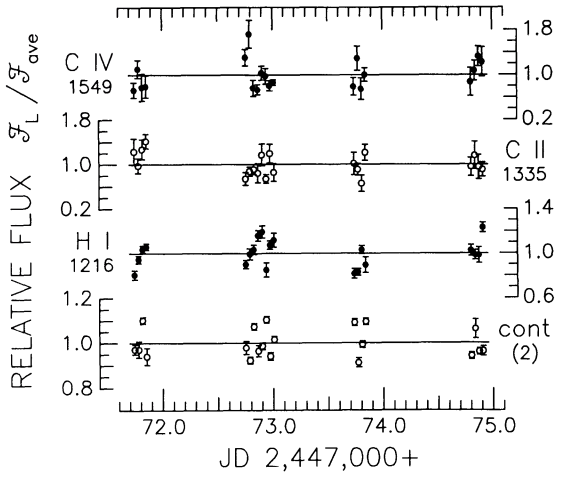

FIG. 3c

FIG. 3.—(*a*) Time series of representative bright far-ultraviolet emissions of Capella. A correction for the thermal response of the SWP camera has been applied, and in all cases the fluxes are depicted relative to the average of the set. The diagnostics are arranged from top to bottom in order of decreasing excitation. The lower panel shows the behavior of the (control) photospheric continuum, an average of three independent 50–100 Å line-free bands: the error bars are the standard errors of the mean. In the other cases, the (1 σ) error bars are derived from a comparison of the rms deviation of the spectral fluxes from the fitted Gaussian line shapes. (*b*) Same as (*a*), but for Procyon; two bands were averaged for the continuum flux. (*c*) Same as (*a*), but for Caph; two bands were averaged for the continuum flux.

the lines and continuum bands that were measured. The continuum bands provide a control check on possible instrumental sensitivity variations.

Figures 3*a*–3*c* illustrate time series of the most prominent emissions in the far-ultraviolet spectra of the three stars. I applied a correction of 0.49% $(°C)^{-1}$ (Holm 1982) to compensate for the thermal response of the SWP camera. Table 6 lists the mean absolute fluxes, the sample standard deviations of the emissions ("σ_{rms}"), and the typical values of the estimated measurement errors ("$\langle\sigma_L\rangle$"). Also included are the maximum rotational modulations of solar far-ultraviolet emission lines (and one 50 Å continuum band) recorded near the peak of sunspot cycle 21 by the *Solar Mesosphere Explorer* (Bennett 1987).

3.3. *Processing and Co-adding the SWP Echelle Spectra*

I processed and co-added the selected SWP echellograms of Procyon and Caph using the techniques described (most recently) by Ayres, Jensen, & Engvold (1988, hereafter AJE). I registered the five nearly optimum spectra of Procyon to a common wavelength scale by cross-correlating a sample of narrow well-exposed emission features (AJE). I registered the fainter exposures of Caph, dominated by broad low-contrast emissions, by correcting the processed spectra for the radial velocity of the star (v_r = 11 km s^{-1}), taking into account the additional systematic shift ($\approx$26 km s^{-1}) for the deep off-center exposure.

Figure 4 illustrates representative line profiles from the co-added far-ultraviolet spectra of Procyon and Caph. Also depicted are Gaussian approximations to the same features from the secondary spectrum of Capella based on the literature

TABLE 6

MEASURED LOW-DISPERSION FLUXES

Feature	Capella	Procyon	Caph	Sun[a]
	Mean Fluxes (10^{-12} ergs cm^{-2} s^{-1})			
Continuum	340	530	150	...
H I λ1216	...	61.7	18.9	...
N V λ1240	6.3	...	...	...
O I λ1305	33.4	4.9	...	...
C II λ1335	24.2	6.7	1.8	...
Si IV λ1400	20.5	...	...	...
C IV λ1549	44.1	10.0	2.6	...
	Standard Deviations σ_{rms} ($\langle\sigma_L\rangle$) (%)			
Continuum	2.5 (0.9)	2.0 (0.5)	6.3 (1.6)	11 (2)[b]
H I λ1216	...	4.5 (2.8)	12.1 (4.6)	21 (2)
N V λ1240	13.9 (10.9)	...	...	...
O I λ1305	4.7 (1.8)	17 (12)	...	40 (20)
C II λ1335	7.8 (2.8)	10 (7)	20 (16)	28 (6)
Si IV λ1400	5.5 (3.6)	...	...	33 (8)
C IV λ1549	5.4 (2.0)	15 (10)	26 (17)	30 (5)

NOTE.—Entries consisting of three dots indicate that the feature was overexposed or too faint to measure; σ_{rms} is the standard deviation of the fluxes in a time series, normalized to the mean flux; $\langle\sigma_L\rangle$ is the average of the assigned measurement uncertainties for that time series.

[a] Near peak of solar cycle 21; Bennett 1987.

[b] 1435±25 Å.

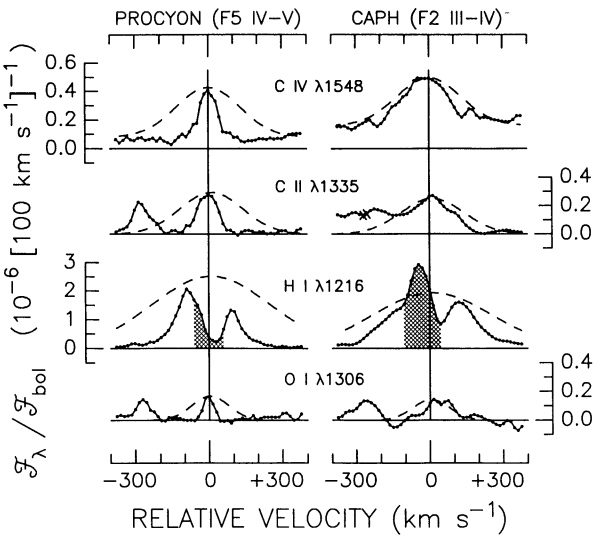

FIG. 4.—Comparison of line shapes of selected far-ultraviolet emissions of the three stars. New co-added *IUE* high-dispersion spectra of Procyon (*left-hand panel*) and Caph (*right-hand panel*) are compared with Gaussian approximations to the line shapes of the Capella secondary (*dashed curves*) as taken from previous work, and scaled to the approximate peak fluxes of the new spectra. The ordinate is a normalized monochromatic flux commensurate in units with the abscissa, a relative velocity scale. Note the compressed flux scale for the bright Lyα feature. The shaded areas in the cores of the Lyα profiles indicate portions of the spectra affected by geocoronal contamination (which almost completely fills in the central interstellar H I absorption of Caph). The features are arranged from top to bottom in order of decreasing excitation. Crosses mark a portion of the short-wavelength component of C II which is affected by an incompletely removed reseau. The spectra were smoothed, for display purposes, by a triangular filter comparable in width to the spectral resolution element (≈25 km s^{-1}) for Procyon, and twice that for the broader, lower contrast emissions of Caph. The H I Lyα and O I λ1306 spectra are weighted averages of the adjacent echelle orders in which each feature is repeated. The velocity scale of the Procyon spectra is registered to the mean of a group of low-excitation chromospheric emissions. A comparable reference sample was not available for Caph: its spectra are displayed in a "predicted" photospheric velocity frame (see text).

previously cited. Table 7 summarizes the line-shape parameters of all features which could be measured with even minimal confidence.

4. ASSESSMENT OF ULTRAVIOLET VARIABILITY

4.1. *Qualitative Description*

4.1.1. *Capella*

The broad-band continuum intensities of Capella—dominated entirely by the warmer secondary—exhibit a vaguely rhythmic progression: the rms is 2.5% compared with the average standard error (among the three independent 50–100 Å intervals) of 0.9%.

The low-excitation chromospheric feature O I λ1305 displays variability of ≈5% rms—approximately twice the expected measurement uncertainty—which is roughly correlated with the ultraviolet continuum. Intermediate-excitation C II λ1335 exhibits a quasi-periodic variation, similar to that of O I but somewhat larger in amplitude. C II is a key indicator because it is bright, relatively isolated, suffers no major blends, and exhibits high contrast with respect to the surrounding continuum (mostly long-wavelength scattered light). The high-temperature emissions Si IV λ1400 and C IV λ1549 vary with about the same amplitude as O I λ1305, at about the same

TABLE 7

MEASURED HIGH-DISPERSION LINE PARAMETERS

A. PROCYON

Transition	$v_L - v_{low\text{-}ex}$	FWHM	f_L	f_C
Low-Excitation Lines: $v_{low\text{-}ex} = 0 \pm 1$				
O I λ1302	+5 ± 1	77	23 ± 1	...
O I λ1304[a]	−1 ± 1	60	17 ± 1	...
O I λ1306[a,b]	−2 ± 2	50	16 ± 2	...
O I λ1306[a,b]	−4 ± 1	69	26 ± 1	...
Cl I λ1351[a]	+4 ± 1	70	14 ± 1	...
O I] λ1355[a]	+6 ± 4	49	6 ± 1	...
Moderate-Excitation Permitted Lines: $\langle v_L \rangle - v_{low\text{-}ex} = -3 \pm 2$				
Si III λ1206[a]	−8 ± 2	110	62 ± 4	...
H I λ1216[b]	−9 ± 1	173	1150 ± 20	...
H I λ1216[b]	−12 ± 1	197	1280 ± 4	...
C II λ1334	−1 ± 1	83	43 ± 1	...
C II λ1335[a]	−2 ± 1	95	54 ± 2	...
He II λ1640	−10 ± 2	62	7 ± 1	55
High-Excitation Intersystem Lines				
O V] λ1218	+1 ± 3	115	18.9 ± 1.4	...
High-Excitation Permitted Lines: $\langle v_L \rangle - v_{low\text{-}ex} = +10 \pm 2$				
N V λ1238	+25 ± 6	122	16 ± 2	...
N V λ1242	+13 ± 3	77	7 ± 1	...
Si IV λ1393[a]	+12 ± 1	91	26 ± 1	9
Si IV λ1402[a]	+10 ± 1	54	8 ± 1	6
C IV λ1548[a]	+2 ± 1	74	50 ± 3	29
C IV λ1550[a]	+4 ± 2	61	21 ± 2	29

B. CAPH

Transition	$v_L - v_r$	FWHM	f_L	f_C
Low-Excitation Lines: $v_{low\text{-}ex} = +30 \pm 3$				
O I λ1304[a]	+20 ± 7	170	6 ± 1	...
O I λ1306[a,b]	+48 ± 9	110	5 ± 1	...
O I λ1306[a,b]	+31 ± 4	180	9 ± 1	...
Moderate-Excitation Permitted Lines				
H I λ1216[b]	+13 ± 3	270	251 ± 9	...
H I λ1216[b]	+7 ± 2	330	255 ± 4	...
C II λ1335	+14 ± 3	210	17 ± 1	...
High-Excitation Intersystem Lines				
O V] λ1218	−30 ± 4	220	11 ± 1	...
High-Excitation Permitted Lines: $\langle v_L \rangle = -6 \pm 11$				
Si IV λ1393[a]	−11 ± 2	220	16 ± 1	...
C IV λ1548[a]	−11 ± 3	220	24 ± 1	10
C IV λ1550[a]	+53 ± 8	290	19 ± 2	10

NOTES.—Line parameters were determined by a least-squares Gaussian modeling procedure. Errors are based on variance of the fitted profile from the true data points. The uncertainty in the FWHM is approximately twice that of the associated line position (expressed as a velocity). Velocities and FWHMs are in km s^{-1}. Line fluxes (f_L) are in units of 10^{-13} ergs cm^{-2} s^{-1} at Earth; continuum fluxes (f_C) are in units of 10^{-13} ergs cm^{-2} s^{-1} $Å^{-1}$ at Earth. Fractional values were rounded.

[a] Lines included in *velocity* average over that excitation group: the weighting was according to *unrounded* $(f_L/\sigma_f)^2$. The uncertainty cited for the differential velocity $\langle v_L \rangle - v_{low\text{-}ex}$ is the quadratic sum of the standard errors of the two quantities.

[b] H I Lyα and O I λ1306 repeat in adjacent echelle orders (114/113, 106/105, respectively): thus, two separate measurements are given.

(low) level of significance with respect to the predicted measurement errors.

While some of the emission variations appear to be correlated in formation temperature and superficially cyclical, the amplitudes are quite small compared with the rotational modulations observed on the Sun (Table 6), a relatively *inactive* star even near the peak of its magnetic cycle.

4.1.2. *Procyon*

The dual continuum bands exhibited variations at the 2% level, somewhat smaller than the continuum of Capella but more significant (4 σ) with respect to the estimated measurement errors. The mostly small differences between continuum fluxes recorded on the same day tend to support the estimated measurement uncertainties. Thus, the continuum variations might be genuine. At the same time, the small rms of the Procyon continuum provides some confidence that the instrument itself was stable over the period of the campaign.

The H I Lyα emission of Procyon varied as much (or as *little*, depending on one's perspective) as the O I λ1305 emission of Capella (rms $\approx$ 5%), but less than 2 σ in significance with respect to the measurement uncertainties, and without any hint of repetitive behavior. The higher excitation emissions—C II and C IV—showed larger fluctuations than Lyα, but not inconsistent with steady behavior given the relative faintness of the two features (compared with Lyα) and the fact that C IV sits on top of a relatively bright photospheric continuum (the correction for which introduces an additional source of noise: see, e.g., Bennett & Ayres 1988).

The rotational period of Procyon probably is about 20 days, so the existing time series is not useful for establishing *persistent* periodicities of the chromospheric Lyα emission. Nevertheless, to the extent that the epoch of the *IUE* campaign is representative of the typical behavior of the subgiant, the rms amplitude of any rotational modulations must be quite small. The implication is that despite the higher surface flux densities of Procyon compared with the Sun, the activity must be distributed much more uniformly with longitude on the subgiant: in the solar case, rotational modulations of Lyα can exceed 20% rms near the peak of the sunspot cycle (Table 6).

4.1.3. *Caph*

Caph exhibits substantially larger variations in its continuum and line emissions than Procyon. While C IV is compromised by its faintness and the elevated photospheric continuum at 1550 Å, the isolated bright Lyα feature should be reliable. The latter appears to change by large amounts on time scales of hours (cf. Ayres & Bennett 1987). Nevertheless, the overall behavior on rotational time scales ($P_{\rm rot} \lesssim 3$ days) appears to be steady.

4.2. *Quantitative Evaluation: Periodogram Analysis*

I evaluated the ultraviolet time series using the "periodogram" technique described by Scargle (1982), as clarified by Horne & Baliunas (1986, hereafter HB): it is well suited to unevenly spaced data strings, and provides a straightforward prescription for evaluating the significance of peaks in the power spectrum. Figures 5*a*–5*c* illustrate periodograms for the three stars: for the continuum; a chromospheric emission (H I or O I); and C II λ1335. I calculated the periodograms for a range of test periods near the known rotational cycles of Capella and Procyon, and the δ Sct pulsational cycle of Caph. Each diagram contains a reference power spectrum of a pure sine wave at the predicted modulation period, averaged over many trials (with random phases) sampled with the same cadence as the real time series. The periodogram of the discretely sampled sinusoid helps one identify artifacts traceable to the *window function* of each sample.

Before calculating the periodogram, I divided the time series by its standard deviation (cf. HB). With that normalization, the "false-alarm probabilities" of Scargle (1982), which are used to deduce statistical significance, depend only on the number of "independent frequencies," $\mathcal{N}_i$, in the data string. I conservatively chose the latter to be the total number of samples, $\mathcal{N}$, in each series rather than $\mathcal{N}/2$ as advocated by Scargle, because the numerical simulations of HB demonstrate that $\mathcal{N}_i \approx \mathcal{N}$ is more appropriate for data strings (like the present ones) where the samples are relatively regularly spaced.

A more judicious evaluation of the significance levels would be warranted (e.g., Koen 1990), if the periodograms had displayed any prominent peaks. In only one case is the power spectrum worthy of further consideration—the far-ultraviolet continuum of Caph with respect to the *pulsation* period. In none of the other cases would any of the apparent peaks attain a minimal 3 σ significance, even with a drastic reduction in the $\mathcal{N}_i$ criterion. While the existence of weak peaks in the periodograms of Capella confirms the qualitative impression of quasi-periodic behavior, the low levels of significance demonstrate that the variability is not *persistently cyclic*. It therefore fails the test of rotational modulations as recorded on the cooler stars, from the Sun to the RS CVn variables.

Thus, *no significant periodic modulations appear in the chromospheric emissions of any of the program stars.*

5. DISCUSSION

5.1. *The Variability of the Ultraviolet Continuum of Caph*

Figure 6 illustrates the ultraviolet continuum (and H I Lyα) of Caph phased according to the $P = 0.101$ days adopted by Teays et al. (1989; the authors monitored the Mg II emission of Caph with the *IUE* about a month after my observing program), and a zero epoch (maximum visual light) of JD 2,447,072.838 $\pm$ 0.003, as measured at McDonald Observatory during the *IUE* campaign (communicated by S. L. Hawley 1987).

On the one hand, the ultraviolet continuum shows an unmistakable sinusoidal variation of amplitude about 10% (0.1 mag) which peaks about 0.1 in phase before maximum visual light. It is known from multicolor studies of the δ Scuti variables that the surface temperature peaks slightly before maximum light (Breger 1979): the far-ultraviolet continuum should be an excellent proxy for temperature in such stars.

On the other hand, while Lyα shows a trend of elevated intensity between phases 0.25 and 0.75 compared with the phases around maximum light—similar to the behavior of the Mg II emission suggested by Teays et al. (1989)—the periodogram analysis indicates that the chromospheric emission is not persistently correlated with the δ Sct cycle. The Lyα flux, although affected slightly by the uncertain correction for geocoronal light, should be a much more reliable tracer of the chromospheric response to pulsational heating than the Mg II doublet: the latter is a low-contrast feature in the early F stars, and its measurement in LWP echellograms is subject to a variety of uncertainties (see Teays et al.). I conclude that there is no hard evidence for a direct connection between the chromospheric variability of Caph and its δ Sct pulsation. Nevertheless, the occasional rapid flux variations seen in Lyα are intriguing and remain to be clarified.

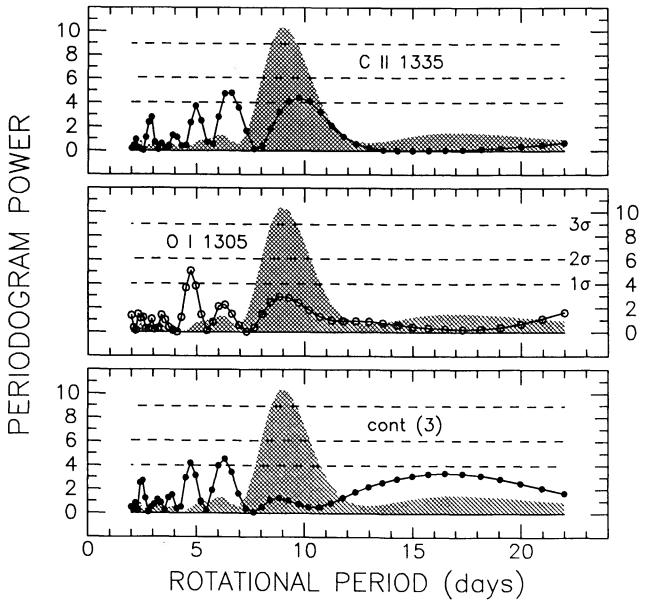

FIG. 5a

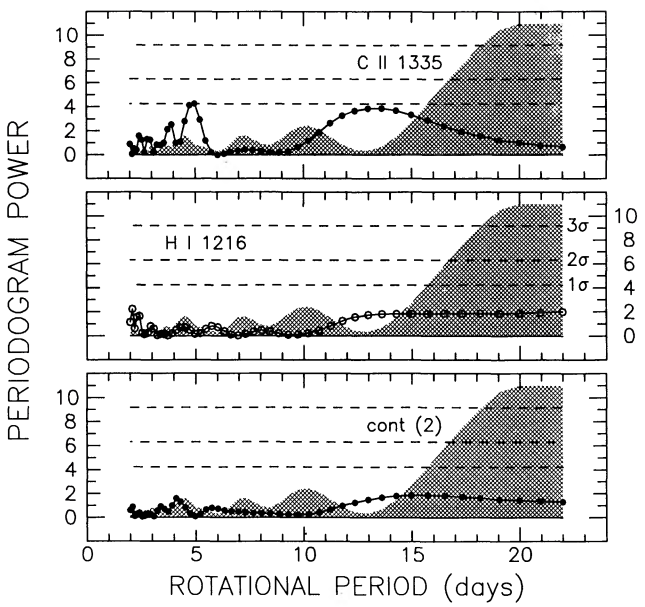

FIG. 5b

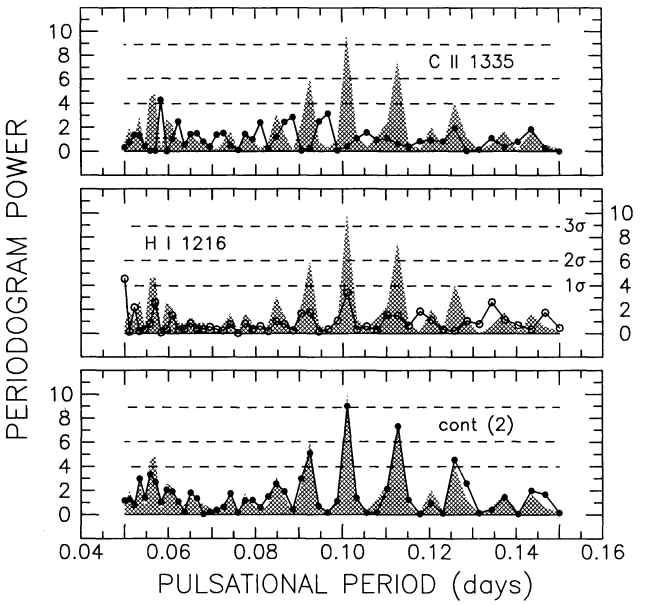

FIG. 5c

FIG. 5.—(*a*) Periodograms of selected time series of Capella. Power spectra of the *IUE* fluxes are depicted with connected filled circles. The hatched area in each panel illustrates the power spectrum expected for a pure sinusoid at the predicted modulation period ($P_{rot} \approx 9$ days), sampled in the same way as the true data. The reference sinusoid illustrates the influence of the sampling "window" on a pure signal, particularly the sidelobe structure. The horizontal dashed lines indicate the significance of a peak with respect to the false-alarm probability as defined by Scargle (1982) and clarified by Horne & Baliunas (1986). The most commonly occurring peaks are at 5, 6.5, and 9–10 days. However, none of the peaks achieves a significance as high as 2 σ, and the indicated amplitudes are well below the modest rotational modulations of even an inactive star like the Sun. (*b*) Same as (*a*), but for Procyon. There are no significant peaks at short periods, and no hint of any upturns near the predicted rotational period of 23 days. Because the duration of the campaign was comparable to the predicted modulation period, the time series cannot reveal persistent cyclical variations. Nevertheless, there certainly is no evidence for even a single cycle of systematic variation. (*c*) Same as (*a*), but for Caph, and calculated with respect to the δ Sct pulsational period of 0.101 days. The periodogram of the pure sinusoid illustrates the severe sidelobes caused by the gaps in the time series dictated by the scheduling of the *IUE* observations during US2 shifts. The modulation of the continuum is highly significant ($\gtrsim 3$ σ) with respect to the false-alarm probability, while Lyα and C II fail to show any significant peaks.

5.2. *Significance of the Line Widths*

Although all three stars are unanimously "nonsolar" with regard to their lack of significant rotational modulations, clear differences are seen among them in their far-ultraviolet emission-line *profiles*.

The high-excitation emissions of Procyon are relatively sharp compared with the broad features of Capella and Caph, particularly the C IV doublet. The average FWHM of the C IV components in the subgiant is only about 25% larger than that measured in five quiet and active G–K *dwarf* stars (Ayres et al. 1983a). The associated nonthermal Doppler broadening of the high-excitation lines of Procyon thus can be only slightly larger than in solar-type dwarfs (where ξ_t is approximately sonic), while the densities in the line-forming layers very likely are much less (cf. Jordan et al. 1987). Accordingly, the maximum flux of pure sound waves passing through the C IV zone must be smaller in the subgiant than in the solar-type dwarfs. Thus, the possibility of heating the overlying corona by acoustic energy is as remote as it is believed to be in the well-studied case of the Sun (Athay & White 1978). That difficulty with the acoustic-corona hypothesis for the "borderline" case of Procyon was readily acknowledged by SD, and no counter-argument was offered by the authors.

The excessive broadening of the C IV emissions of Capella and Caph contrasts sharply with the narrow lines of Procyon. The two giant stars are fast rotators, but rotational broadening in and of itself should produce a feature of only about *half* the observed width, even if the C IV emission is optically thick and

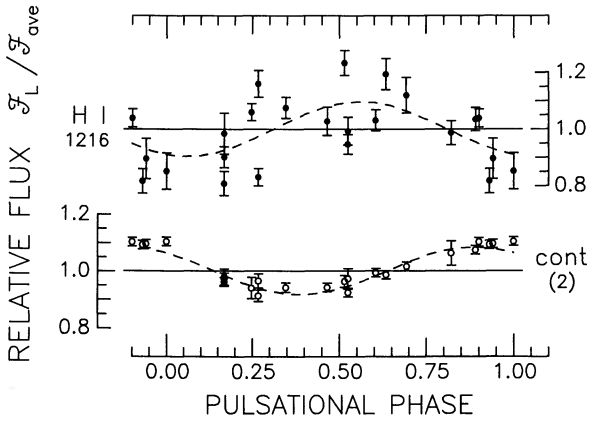

FIG. 6.—The Caph time series of Fig. 3*c*, phased according to the 0.101 day δ Sct pulsational cycle. The clearly rhythmic variation of the far-ultraviolet continuum peaks about 0.1 cycles before maximum light ($\phi \equiv 0$, established on the basis of contemporaneous optical photometry); consistent with the previously inferred behavior of the surface temperature (for which the ultraviolet continuum is an excellent proxy). The chromospheric H I Lyα emission shows a mild tendency to be elevated around the time of *minimum* light compared with the phases near maximum light; a similar behavior has been reported for the chromospheric Mg II λ2800 emission of Caph. However, the periodogram analysis indicates that Lyα is not *persistently* periodic on the pulsational cycle.

the nonthermal Dopper velocities are mildly supersonic. One possibility is that the large-scale velocity fields in the outer atmospheres of both stars are *hyper*sonic, and completely dominate the broadening of the high-excitation emissions. Another possibility is that the 10^5 K gas resides in vertically extensive structures that corotate with the surface, thereby amplifying the rotational broadening. If that is the case, the C IV–emitting plasma must be in a transitory dynamic state because the pressure scale height at 10^5 K is too small to support hydrostatic gas a significant fraction of a stellar radius above the surface. Furthermore, one must explain why the lines of Caph are somewhat narrower than those of the Capella secondary, while the v sin i of Caph is 40% larger. Unfortunately, one cannot base any firm conclusions on the existing sample of only two Hertzsprung gap stars.

5.3. *Significance of the Line Shifts*

Nevertheless, an additional clue is available through the line *shifts*. Many late-type stars—Capella is the prototype—display small but statistically significant *redshifts* of their Si IV and C IV resonance lines with respect to lower excitation chromospheric features (as most recently discussed by AJE). The shifts are thought to indicate *downflows* of hot gas like those commonly seen in coronal magnetic loops on the Sun.

It is perhaps significant, therefore, that the co-added spectra of Procyon show positive evidence for high-excitation redshifts (specifically the Si IV doublet), whereas the high-excitation species of Caph not only are *not* redshifted but show a 3 σ *blueshift* (-36 ± 11 km s^{-1}) with respect to the low-excitation oxygen triplet. Unfortunately, the poor quality of the *IUE* spectra of Caph precludes a definitive assessment. One worrisome problem is that the low-excitation lines themselves show a 30 km s^{-1} *redshift* with respect to the predicted radial velocity of the star. An instrumental error of that magnitude occurring simultaneously in three independent echellograms would be unprecedented. Conceivably the O I lines might be strongly red-asymmetric owing to *outflows* in the upper chromosphere of the sort envisioned by SD, and thus should not be utilized as a fiducial for the stellar rest velocity. Instead, one should consider the velocity of the high-excitation lines with respect to the predicted v_r of Caph: in that light the Si IV and C IV lines fall essentially at the photospheric velocity. (Note: the large standard error of the weighted average is dominated by the low-significance, ostensibly inconsistent C IV λ1550.8 component.) Incidentally, a marginally significant feature appears in the long-wavelength wing of Lyα at the expected location of O V] λ1218.4. If real, it would be the highest excitation emission ($\approx 2 \times 10^5$ K) identifiable in the co-added far-ultraviolet spectrum of Caph, and it displays a significant *blueshift* of about 30 km s^{-1} in the photospheric reference frame.

5.4. *Does "Nonsolar" Truly Signify Acoustic?*

While the far-ultraviolet and X-ray emission properties of stars on either side of the "acoustic/magnetic" boundary are distinct, that should not be construed as evidence that the coronal heating mechanism must be exclusively acoustic on the one side and exclusively magnetic on the other. It is quite possible, as emphasized by Giampapa & Rosner (1984), that coronae (and chromospheres) on the warmer side of the boundary are energized simply by a different type of magnetic activity than that which appears to dominate the cooler side: the thin, but turbulent, convection zones of the F-type stars might produce substantial magnetic flux, but perhaps lacking the high degree of spatial organization, and long-term cyclical behavior, conferred by a solar-type dynamo.

On the other hand, even on the "magnetic" side of the boundary a relatively large proportion of the low-excitation Ca II and Mg II emission from quiet stars like the Sun appears to arise in a "basal" chromosphere (e.g., Schrijver 1987), whose strength is independent of rotation (and thus likely derives from a nonmagnetic heating mechanism).

6. SUMMARY AND CONCLUDING REMARKS

Far-ultraviolet spectroscopy reveals intriguing similarities between the "F" stars Capella, Procyon, and Caph, but puzzling differences that are difficult to reconcile with the placement of all three on the acoustic side of the SD boundary.

On the one hand, none of the stars show any significant rotational modulations of their chromospheric emissions, suggesting that their surface "activity" is uniformly dispersed—in keeping with the acoustic scenario—rather than concentrated into activity "patches" as in cooler stars like the Sun (cf. Toner & Gray 1988). Caph does not exhibit significant redshifts of its high-excitation species, the positive detection of which has been linked to solar-like magnetic activity in cooler stars (particularly the Capella secondary). Instead, Caph exhibits marginal, but nonetheless tantalizing, evidence for red asymmetries in its low-excitation lines and/or blueshifts of its high-excitation lines. In either case, the associated outflows, if real, would provide some support for the acoustic-wave–driven coronal mass-loss scenario that SD invoke to explain the striking X-ray deficiencies of the early F stars and related objects.

To balance the subtle—but ostensibly opposed—behaviors of Caph and the Capella secondary in their global gas dynamics, the excessive widths of the high-excitation lines of the δ Sct star are curiously similar to those of the cooler, more luminous giant. Whether the similarity is significant or coincidental cannot be assessed at present because the number of examples is restricted at present to the two prototypes. Little

additional progress can be expected from the *IUE* because it is not sensitive enough to reach the next tier of fast-rotating Hertzsprung gap giants. On the other hand, the Goddard High Resolution Spectrograph of the *Hubble Space Telescope* (*HST*) will be able to reach many tens of stars near the SD boundary, at higher dispersion and with better signal-to-noise ratio than the *IUE*.

Thus the present work should be viewed as a progress report concerning an issue whose resolution lies in the future. Indeed, the global problem of chromospheric heating across the H-R diagram in many ways is like that which confronts solar physicists: no single simple theory can readily explain the sometimes subtle, sometimes vivid structure that is seen. Perhaps as our view of the stars becomes more "solar-like," with the advent of *HST*, we will uncover a profound connection between the curious boundaries in spectral type and luminosity—where the manifestations of chromospheric heating undergo fundamental transformations—and the dazzling array of fine structure that so ubiquitously mottles the Sun's surface.

This work was supported by the National Aeronautics and Space Administration through grants NAG5-199 and NAG5-1215 to the University of Colorado. I thank S. Hawley for coordinating the optical photometry of Caph during the *IUE* campaign, and S. Baliunas for helpful discussions concerning the practical application of the periodogram analysis.

REFERENCES

Altner, B. 1988, NASA IUE Newsletter, No. 37, p. 43
Athay, R. G., & White, O. R. 1978, ApJ, 226, 1135
Ayres, T. R. 1975, Ph.D. thesis, Univ. of Colorado
———. 1984, ApJ, 284, 784
———. 1988, ApJ, 331, 467
———. 1990, PASP, 102, 1420
Ayres, T. R., & Bennett, J. O. 1987, in Lecture Notes in Physics, Vol. 274, Stellar Pulsation, ed. A. N. Cox, W. M. Sparks, & S. G. Starrfield (New York: Springer-Verlag), 127.
Ayres, T. R., Jensen, E., & Engvold, O. 1988, ApJS, 66, 51 (AJE)
Ayres, T. R., Judge, P., Jordan, C., Brown, A., & Linsky, J. L. 1986, ApJ, 311, 947
Ayres, T. R., & Linsky, J. L. 1980, ApJ, 241, 279
Ayres, T. R., Linsky, J. L., & Shine, R. A. 1974, ApJ, 192, 93
Ayres, T. R., Linsky, J. L., Simon, T., Jordan, C., & Brown, A. 1983a, ApJ, 274, 784
Ayres, T. R., Marstad, N. C., & Linsky, J. L. 1981, ApJ, 247, 545
Ayres, T. R., Schiffer, F. H., III, & Linsky, J. L. 1983b, ApJ, 272, 223
Bagnuolo, W. G., Jr., & Sowell, J. R. 1988, AJ, 96, 1056
Beasley, A. J., & Cram, L. E. 1990, Solar Phys., 125, 191
Bennett, J. O. 1987, Ph.D. thesis, Univ. of Colorado
Bennett, J. O., & Ayres, T. R. 1988, PASP, 100, 1129
Breger, M. 1979, PASP, 91, 5
Coleman, C., & Snijders, T., eds. 1977, *IUE* Technical Note, No. 31
Dravins, D., Lind, J., & Särg, K. 1977, A&A, 54, 381
Fracassini, M., Pasinetti, L. E., Castelli, F., Antonello, E., & Pastori, L. 1983, Ap&SS, 97, 323
Giampapa, M. S., & Rosner, R. 1984, ApJ, 286, L19
Gray, D. F. 1967, ApJ, 149, 317
———. 1981, ApJ, 251, 152
Harris, A. W., & Sonneborn, G. 1987, in Exploring the Universe with the *IUE* Satellite, ed. Y. Kondo (Dordrecht: Reidel), 729
Hoffleit, D., & Jaschek, C. 1982, The Bright Star Catalogue (4th ed.; New Haven: Yale University Observatory)
Hollars, D. R. 1974, ApJ, 194, 137
Holm, A. V. 1982, NASA *IUE* Newsletter, No. 18, p. 10
Horne, J. H., & Baliunas, S. L. 1986, ApJ, 302, 757 (HB)
Jordan, C., Ayres, T. R., Brown, A., Linsky, J. L., & Simon, T. 1987, MNRAS, 225, 903
Jordan, C., & Linsky, J. L. 1987, in Exploring the Universe with the *IUE* Satellite, ed. Y. Kondo (Dordrecht: Reidel), 259
Koen, C. 1990, ApJ, 348, 700
Kraft, R. P. 1957, ApJ, 125, 336
Landman, D. A., Roussel-Dupré, R., & Tanigawa, G. 1982, ApJ, 261, 732 (LRT)
Linsky, J. L. 1988, in Multiwavelength Astrophysics, ed. F. A. Córdova (New York: Cambridge Univ. Press), 49
Linsky, J. L., & Marstad, N. C. 1981, in The Universe at Ultraviolet Wavelengths: The First Two Years of *IUE*, ed. R. Chapman (NASA CP-2171), 287
McNamara, D. H., & Augason, G. 1962, ApJ, 135, 64
Millis, R. L. 1966, Inf. Bull. Var. Stars, No. 137
Noyes, R. W., Hartmann, L., Baliunas, S. L., Duncan, D. K., & Vaughan, A. H. 1984, ApJ, 279, 763
Parker, E. N. 1970, ARA&A, 8, 1
Rucinski, S. M. 1986, in Lecture Notes in Physics, Vol. 254, Cool Stars, Stellar Systems, and the Sun, ed. M. Zeilik & D. M. Gibson (New York: Springer-Verlag), 307
Scargle, J. D. 1982, ApJ, 263, 835
Schmidt, E. G., & Parsons, E. B. 1984, ApJ, 279, 202
Schrijver, C. J. 1987, A&A, 172, 111
Simon, T., & Drake, S. A. 1989, ApJ, 346, 303 (SD)
Slettebak, A., Collins, G. W., II, Boyce, P. B., White, N. W., & Parkinson, T. D. 1975, ApJS, 29, 137
Smith, M. A. 1979, PASP, 91, 737
Strand, K. Aa. 1951, ApJ, 113, 1
Teays, T. J., Schmidt, E. G., Fracassini, M., & Pasinetti Fracassini, L. E. 1989, ApJ, 343, 916
Toner, C. G., & Gray, D. F. 1988, ApJ, 334, 1008
Ulmschneider, P. 1979, Space Sci. Rev., 24, 71
Walker, H. J., & Wolstencroft, R. D. 1988, PASP, 100, 1509
Walter, F. M. 1983, ApJ, 274, 794
Wolff, S. C., Boesgaard, A. M., & Simon, T. 1986, ApJ, 310, 360